

This is the author's peer reviewed, accepted manuscript. However, the online version of record will be different from this version once it has been copyedited and typeset.

PLEASE CITE THIS ARTICLE AS DOI: 10.1063/1.50240101

New insights into impact-induced removal of the deposited droplet

Fangfang Xie (解芳芳)^a, Hongzeng Xin (辛洪增)^a, Qianyi Liu (刘钱艺)^a, Zhiyin Yang^b, Amirali Shateri^b, Wenpeng Hong (洪文鹏)^a and Mingjun Liao (廖明俊)^{a,*}

^a School of Energy and Power Engineering, Northeast Electric Power University, Jilin, 132012,
China

^b School of Engineering, University of Derby, DE22 3AW, United Kingdom

*Corresponding Author: liaomj666@gmail.com;

Abstract: This paper presents a comprehensive investigation into the collision dynamics of equal and unequal-sized nanodroplets on a flat surface using molecular dynamics (MD) simulations, revealing new insights into scaling laws and energy dissipation mechanisms. The simulations, conducted with the Large-Scale Atomic/Molecular Massively Parallel Simulator (LAMMPS) software, involved an initially stationary droplet on the surface and a suspended droplet with varying diameter ratios (λ) and impact velocities. The results show that at low Weber numbers ($We < 24.15$), the droplets tend to deposit after impact, while at higher Weber numbers ($We \geq 24.15$), they undergo spreading and retraction, ultimately rebounding. The study reveals that the dimensionless contact time (t^*) and maximum spreading factor (β^*_{\max}) in collisions between droplets of different sizes do not follow the same scaling relationship observed in single nanodroplet impacts. By redefining the Weber and Reynolds numbers (Re), the new scaling relationships $t^* \sim We^{2/3} Re^{-1/3} \lambda^{-1/3}$ and $\beta^*_{\max} \sim We^{2/3} Re^{-1/3} \lambda^{1/3}$ are proposed and validated. This work represents a further in-depth study of previous research on single nanodroplet impact, introducing for the first time the diameter ratio in unequal droplet impacts into the variation patterns of contact time and maximum spreading diameter. Moreover, these findings highlight the importance of revisiting and potentially revising classical theories to accommodate the unique physical phenomena that emerge at smaller scales.

Keywords: impact; bouncing; diameter ratio; contact time; maximum spreading factor.

1. Introduction

Droplet dynamics, particularly during collision events, are of paramount importance in a wide array of scientific and industrial processes, including inkjet printing,¹ pesticide spraying,² coating technologies,³ and raindrop formation.⁴ These processes demand a precise understanding of droplet

This is the author's peer reviewed, accepted manuscript. However, the online version of record will be different from this version once it has been copyedited and typeset.

PLEASE CITE THIS ARTICLE AS DOI: 10.1063/1.50240101

behavior to optimize efficiency and effectiveness in applications ranging from high-resolution printing to efficient pesticide delivery.^{5,6}

Over the past decades, extensive research has focused on the impact dynamics of a single droplet on solid surfaces, exploring phenomena such as spreading, rebounding, and splashing under varying conditions of surface roughness, wettability, and material properties.^{7,8} For instance, studies by Singh et al.⁹ and Aziz et al.¹⁰ investigated the effects of surface roughness and fibrous structures on droplet impact dynamics, emphasizing the critical role of surface energy dissipation in determining outcomes like rebound and spreading. The different outcomes such as rebounding or spreading under the given conditions are particularly relevant to self-cleaning surfaces and anti-icing technologies, where controlling droplet behavior can significantly enhance performance.

However, the complexity increases significantly when considering binary droplet collisions, which are common in applications such as inkjet printing, where droplets of different sizes, velocities, and compositions frequently interact.^{11,12} Binary droplet collisions introduce additional variables, such as the relative sizes and velocities of the droplets, which can lead to a wide range of outcomes, including coalescence, bouncing, and fragmentation.¹³ Early studies by Brazier-Smith et al.¹⁴ and Estrade et al.¹⁵ provided foundational insights into the outcomes of binary droplet collisions under varying impact conditions, highlighting the significant influence of Weber number and surface tension on the collision behavior. Sommerfeld & Pasternak¹⁶ further extended this understanding by modeling binary droplet collision outcomes in sprays, elucidating the complex interplay between droplet size, velocity, and environmental conditions.

Despite these advances, most research has traditionally focused on macroscopic droplets, which limits our understanding of droplet behavior at the nanoscale.¹⁷ At smaller scales, where droplet sizes

This is the author's peer reviewed, accepted manuscript. However, the online version of record will be different from this version once it has been copyedited and typeset.

PLEASE CITE THIS ARTICLE AS DOI: 10.1063/1.50240101

approach the nanometer range, the influence of viscous forces, surface tension, and intermolecular interactions becomes much more pronounced.¹⁸ Xie et al.¹⁹ demonstrated that nanoscale droplets exhibit significantly stronger viscous effects and higher energy dissipation during impacts, which can drastically alter their dynamic behavior compared with larger, macroscopic droplets. Zhao et al.²⁰ further explored the role of surface chemistry in nanoscale droplet collisions, revealing that even minor variations in surface properties can lead to drastically different outcomes, such as enhanced spreading or suppressed rebound.

The shift from macroscopic to nanoscale droplets necessitates a reevaluation of traditional models that describe droplet collision dynamics.²¹ Classical scaling laws, which have been extensively validated for larger droplets, often fail to accurately predict the behavior of nanoscale droplets due to the increased relevance of surface forces and energy dissipation mechanisms.²² For example, while macroscopic droplet collisions are often governed by inertial forces, nanoscale droplets are more influenced by surface tension and viscosity, leading to unique collision outcomes that are not observed at larger scales.²³ Ren et al.¹³ highlighted this discrepancy by showing that the maximum spreading diameter of binary nanoscale droplets is strongly dependent on both the Weber and Reynolds numbers, as well as the specific material properties of the surface.

In addition to these general observations, specific studies have examined the collision dynamics of unequal-sized droplets, a scenario that is particularly relevant in applications such as inkjet printing and coating processes.^{24,25} Cheng et al.²⁶ conducted numerical simulations to investigate head-on collisions of unequal-sized droplets on superhydrophobic surfaces, finding that size disparities significantly influence the collision outcome, with larger droplets tending to dominate the interaction. Similarly, Qian et al.²⁷ used molecular dynamics simulations to explore the collision behavior of

This is the author's peer reviewed, accepted manuscript. However, the online version of record will be different from this version once it has been copyedited and typeset.

PLEASE CITE THIS ARTICLE AS DOI: 10.1063/1.50240101

micro- and nanoscale droplets, revealing that the size ratio between droplets plays a crucial role in determining the energy conversion and ultimate fate of the droplets after collision.

However, while these studies provide valuable insights, they also underscore the need for more comprehensive models that can account for the wide range of variables influencing nanoscale droplet collisions.^{28,29} This is particularly important given the increasing use of nanoscale droplets in advanced manufacturing processes, such as nanomaterial deposition and drug delivery systems, where precise control over droplet behavior is critical.³⁰ The challenge lies in developing models that can accurately predict the behavior of droplets across different scales and under varying environmental conditions, a task that requires a deep understanding of the underlying physical mechanisms at play.^{31,32}

To address these gaps, the present study employs molecular dynamics (MD) simulations to investigate the collision dynamics of equal and unequal-sized nanodroplets on solid surfaces. By systematically varying impact velocities and droplet size ratios, this research aims to establish new scaling laws that more accurately describe the behavior of nanoscale droplets, particularly in scenarios where traditional macroscopic models fail.³³ The findings from this study are expected to provide critical insights into energy dissipation mechanisms and scaling relationships, offering a more comprehensive framework for predicting and controlling droplet interactions in various applications.

This research builds on the extensive body of work exploring droplet dynamics by extending the investigation into the nanoscale, where new physical phenomena emerge due to the increased influence of surface forces and energy dissipation. By focusing on the collision dynamics of binary nanodroplets, particularly those of unequal size, this study not only contributes to the theoretical

understanding of droplet behavior but also offers practical insights for the design and optimization of advanced technologies that rely on precise control over nanoscale droplet interactions.

2. Model and method

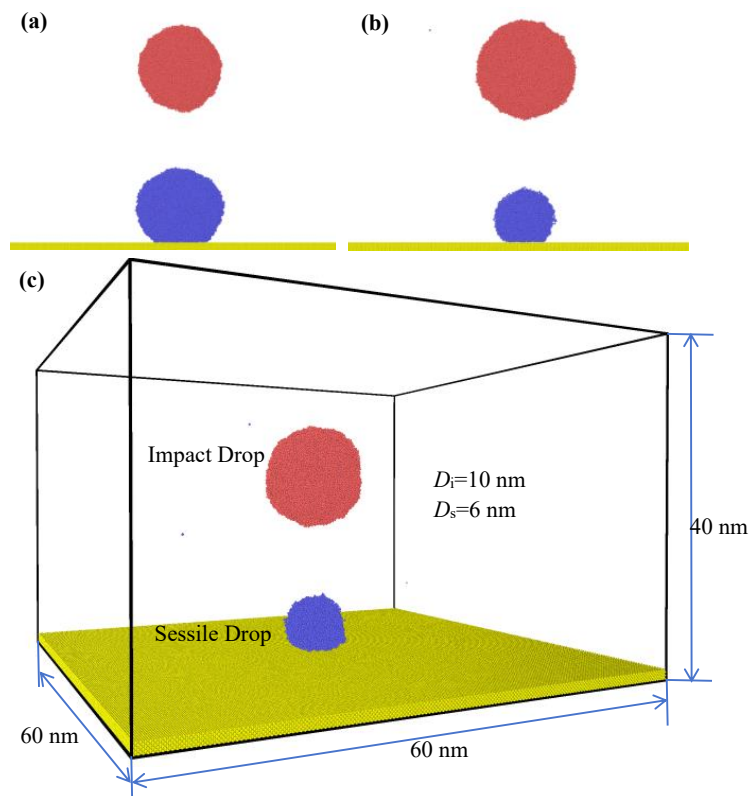


Fig. 1 The initial configuration of the collision of equal (a) and unequal (b) sized nanodroplets, and the simulation system (c).

In this study, MD simulations were conducted using the Large-Scale Atomic/Molecular Massively Parallel Simulator (LAMMPS) to investigate the collision dynamics of equal (Fig. 1a) and unequal (Fig. 1b) sized nanodroplets on a flat surface. The initial configuration of the simulation is shown in Fig. 1c. The simulation box dimensions are set to 60 nm \times 60 nm \times 40 nm, with periodic

This is the author's peer reviewed, accepted manuscript. However, the online version of record will be different from this version once it has been copyedited and typeset.

PLEASE CITE THIS ARTICLE AS DOI: 10.1063/1.50240101

boundary conditions applied in the x and y directions, and a reflective wall in the z direction. It should be mentioned that while this approach provides a controlled environment for studying droplet collisions, it simplifies the complexity of real-world surface chemistries and material heterogeneity. These assumptions are necessary to balance accuracy with computational efficiency, but they may limit the direct applicability of the results to more complex systems. Therefore, if complex system simulation is required, further verification of boundary conditions is needed. The flat surface is located at the bottom of the box and consists of a platinum (Pt) solid with a thickness of 1.17 nm, containing 327,726 Pt atoms. While platinum typically exhibits a lower contact angle due to its high surface energy, in MD simulations, Pt is frequently employed as substrates to achieve the desired contact angle by modifying interaction parameters. This allows researchers to simulate a wide range of surface wettabilities, from hydrophilic to superhydrophobic, by controlling the Lennard-Jones potential between the atoms.^{7,18,22,35} Such flexibility enables the exploration of various droplet behaviors, including those that extend beyond the natural wettability of the surface material. Due to considerations of computational resources, the diameter of the droplet on the flat surface varies, set at $D_s=4$ nm, 6 nm, 8 nm, and 10 nm, and it remains stationary on the flat surface with a contact angle of $\theta=145^\circ$. The diameter of the suspended droplet is fixed at $D_f=10$ nm, where the bottom of the suspended droplet is positioned 2 nm above the top of the stationary droplet. Impact velocities (v_i) for the suspended droplet were selected based on a range of Weber numbers, ensuring a comprehensive exploration of both low and high-energy collision regimes. The simulations followed a two-stage process: initial equilibration and subsequent impact, with detailed attention to energy conservation and distribution to accurately capture the collision dynamics. To prevent deformation of the substrate during the droplet impact, the bottom two layers of Pt atoms are fully fixed with zero force applied,

while the remaining atoms are fixed using virtual springs.

The monatomic water (mW) model³⁴ is used to describe the water molecules, which has been widely employed in studies involving water impact on surfaces.^{7,35-37} The advantage of this model lies in its computational efficiency and ability to accurately reproduce the surface tension, density, and energetics of liquid water compared with traditional water modeling methods. However it should be noted that this model does not account for hydrogen bonding interactions. This omission could influence certain dynamic behaviors, particularly at smaller scales where molecular interactions play a more significant role. Nonetheless, for the scope of this study, which focuses on droplet behaviors like rebound, contact time, and sliding distance, the use of the mW model remains appropriate and does not undermine the validity of the results. The interaction between water molecules is described by the Lennard-Jones 12-6 potential function:³⁸

$$U(r) = 4\epsilon \left[\left(\frac{\sigma}{r} \right)^{12} - \left(\frac{\sigma}{r} \right)^6 \right] \quad (1)$$

where ϵ represents the potential well depth, σ represents the zero-crossing distance, and r is the inter-molecular distance. To save computational resources, the cutoff distance r_{cut} is set to 1 nm, meaning that when $r > r_{\text{cut}}$, the inter-molecular force is negligible, and the potential function is only calculated for distances less than the cutoff distance. Both the Pt plate and water droplets are constructed by face-centered cubic (FCC) with corresponding lattice constants of 0.39 nm and 0.49 nm. The interaction parameters between Pt-Pt atoms are $\epsilon_p = 0.69375$ eV and $\sigma_p = 0.247$ nm, while the interaction parameters between water and Pt are $\epsilon_{w-p} = 0.0051$ eV and $\sigma_{w-p} = 0.28155$ nm. According to Li et al.,³⁷ the density and surface tension of the water molecules are 0.997 g/cm³ and 66 mN/m, respectively, with a viscosity of 283.7 $\mu\text{Pa}\cdot\text{s}$ (the mW model has a viscosity three times lower than the experimental value due to the neglect of hydrogen atom polarization). In the simulations, the time unit is defined

as 1 ps, and a timestep of 2 fs is employed, with the Velocity-Verlet algorithm utilized to solve the Newtonian equations of motion for each atom.

All simulation processes are divided into two stages. The first stage is system equilibration: initially, the system is run in the NVT (canonical) ensemble using the Nose-Hoover thermostat to maintain the temperature at 300 K for 0.6 ns. Then the thermostat is removed, and the system switches to the NVE (microcanonical) ensemble to ensure constant energy, running for an additional 0.4 ns until the system energy stabilizes. During this period, the suspended droplet is fixed at its initial position, allowing only the stationary droplet on the wall to spread in the z direction. After 1 ns of running, the system's energy, temperature, and pressure are uniformly distributed, indicating that the system has reached equilibrium. It is important to note that the stationary droplet remains stable and does not spread uncontrollably during this stage. This is ensured by achieving equilibrium during the initial NVT ensemble equilibration stage. As a result, the droplet maintains its shape and contact angle throughout the simulation. The second stage is the droplet impact stage: in the NVE ensemble, the system energy is maintained constant during the impact process. The suspended droplet is given an initial downward velocity to collide with the stationary droplet. The dynamic evolution process is recorded every 1 ps for subsequent analysis. The Open Visualization Tool (OVITO) software is used for visualization and analysis of the simulation results. After each simulation, the maximum spreading diameter of the droplet is extracted to study the dynamic collision behavior.

3. Verification of the simulation results

3.1 Comparison and validation with experimental results

This is the author's peer reviewed, accepted manuscript. However, the online version of record will be different from this version once it has been copyedited and typeset.

PLEASE CITE THIS ARTICLE AS DOI: 10.1063/1.50240101

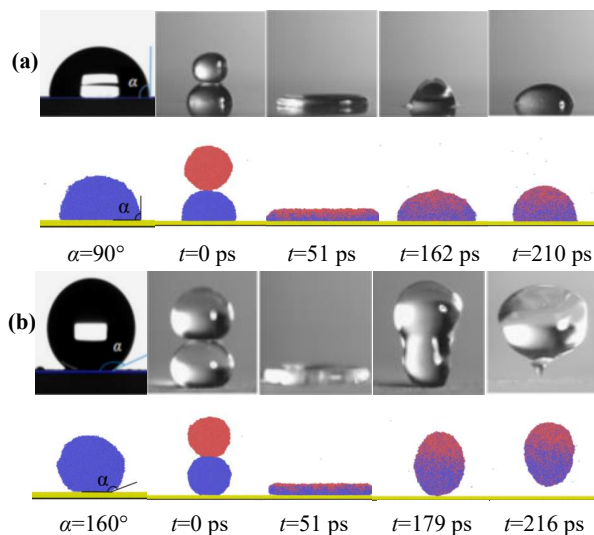


Fig. 2. Comparison of simulation and experimental results³⁹ for binary droplets impacting substrates at different contact angles. (a) Results for a contact angle of 90° ; (b) Results for a contact angle of 160° .

In this study, the MD simulation results were validated against macroscopic experimental data for droplet impact behavior.³⁹ While nanoscale and macroscopic droplet collisions differ significantly in terms of energy dissipation and the influence of surface forces, the fundamental stages of collision, such as spreading, retraction, and rebound, are governed by similar physical principles across scales. Therefore, validating these shared behaviors ensures that the simulation model accurately captures the essential dynamics of droplet impact, even at the nanoscale. The experiment offers a comprehensive analysis of how different wettability characteristics and Weber numbers influence the coalescence dynamics of droplets on solid surfaces. Here numerical simulations using the same parameters as the experiments were conducted to compare with the experimental results of droplet impact at contact angles of 90° and 160° (see Fig. 2). Both the simulation and experimental results

identify four stages in droplet collision: coalescence, spreading, retraction, and deposition/rebound. At a contact angle of 90° , droplets adhere to the substrate during the retraction stage, while at 160° , they completely bounce off. The numerical simulations align perfectly with the experimental observations concerning the deformation characteristics and coalescence from post-collision, thereby confirming the model's accuracy and its potential for predicting nanoscale droplet behaviors.

3.2 Comparison and validation with previous simulation results

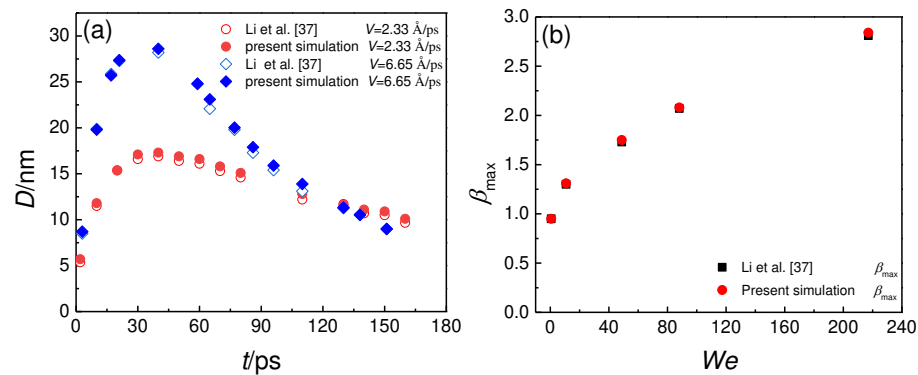


Fig. 3. Temporal evolution of spreading diameter and maximum spreading factor. (a) Evolution of D over time compared with previous studies;³⁷ (b) β_{\max} compared with previous studies.³⁷

To further validate the accuracy of the present model, a series of simulations of nanodroplet impacts on solid surfaces were conducted, and the quantitative results were compared with those of Li et al.³⁷ They studied the spreading and breakup behavior of nanodroplets impacting solid surfaces. Through numerical simulations and experiments, they analyzed the dynamic processes of droplets under different surface conditions, exploring droplet spreading speed, breakup mechanisms, and the influence of surface properties on droplet behavior. The same initial conditions as Ref.³⁷ were used in the present study, including droplet diameter, contact angle, and impact velocity. By comparing the temporal evolution of droplet spreading diameter (D) and maximum spreading factor ($\beta_{\max}=D_{\max}/D_i$,

where D_{\max} is the maximum spreading diameter), it was found that the current simulation results were in excellent agreement with those of Ref.³⁷ as shown in Fig. 3. This comparison demonstrates the high accuracy and reliability of our MD simulation method.

4. Results and discussion

To get further insights into the dynamics of the head-on impact, it is first necessary to understand the forms of energy involved in this process and the corresponding energy conversion processes, which are similar to those described by Wildeman et al.⁴⁰ and Ray et al.⁴¹ The total energy E is composed of four parts: mechanical energy (E_m), surface energy (E_s), viscous dissipation (E_{vis}), and work of adhesion (E_w), expressed as:

$$E = E_m + E_s + E_{\text{vis}} + E_w \quad (1)$$

where $E_m = E_k + E_g$, E_k is the kinetic energy and E_g is the gravitational potential energy. Since this work studies the impact of nano-droplets, gravity can be neglected, so E_m simplifies to E_k .^{37,42} Here, E_k encompasses translational kinetic energy, as well as oscillation and rotational energies. The energy terms can be expressed as follows:

$$E_k = \int_{\Omega} \frac{1}{2} \rho (\mathbf{u} \cdot \mathbf{u}) d\Omega \quad (2)$$

$$E_s = \int_A \gamma dA + \int_{A'} \gamma (1 - \cos \theta) dA' \quad (3)$$

$$E_{\text{vis}} = \int_0^t \left(\int_{\Omega} \phi d\Omega \right) dt \quad (4)$$

$$E_w = \pi \gamma R^2 (1 + \cos \theta) \sin^2 \theta \quad (5)$$

where $d\Omega$ is the differential volume, dA is the surface area at the liquid–gas interface, dA' is the surface area at the liquid–solid interface, and ϕ represents the viscous dissipation rate, given by:

$$\phi = 2\mu \left[\left(\frac{\partial u}{\partial x} \right)^2 + \left(\frac{\partial v}{\partial y} \right)^2 + \left(\frac{\partial w}{\partial z} \right)^2 \right] + \mu \left[\left(\frac{\partial u}{\partial y} + \frac{\partial v}{\partial x} \right)^2 + \left(\frac{\partial v}{\partial z} + \frac{\partial w}{\partial y} \right)^2 + \left(\frac{\partial w}{\partial x} + \frac{\partial u}{\partial z} \right)^2 \right] \quad (6)$$

where u , v , and w are the velocity components in the X , Y , and Z directions, respectively.

This is the author's peer reviewed, accepted manuscript. However, the online version of record will be different from this version once it has been copyedited and typeset.

PLEASE CITE THIS ARTICLE AS DOI: 10.1063/1.50240101

4.1 Impact of equal-sized droplets

The impact dynamics of equal-sized nanodroplets were first examined under varying We numbers, revealing significant differences in behavior across different energy regimes. Fig. 4 illustrates the impact process of two droplets, each with a diameter of 10 nm, at We numbers of 1.5, 73.9, 150.9, and 217.3. It has been found that at $We < 24.15$, the droplets tend to deposit on the surface after collision, primarily due to insufficient kinetic energy to overcome the viscous dissipation during the impact process. This is consistent with previous findings where low-energy collisions are dominated by viscous forces, leading to energy dissipation rather than rebounding.¹³ As We increases ($We \geq 24.15$), the droplets transition from deposition to rebound, demonstrating more significant spreading and retraction phases. The conversion of kinetic energy into surface energy and its subsequent re-conversion during retraction plays a critical role in determining whether the droplet will rebound or not.^{9,19,43-51} Taking Fig. 4b as an example, 0-56 ps is the spreading phase of the droplets. During this process, both the falling and the sessile droplets deform and spread rapidly until they reach the maximum spreading state, converting the kinetic energy of the falling droplet into the surface energy of the two droplets. During the subsequent retraction and rebound phase (56-248 ps), the surface energy stored in the two droplets is gradually released, converting back into kinetic energy, causing the merged droplets to bounce off the surface.

This is the author's peer reviewed, accepted manuscript. However, the online version of record will be different from this version once it has been copyedited and typeset.

PLEASE CITE THIS ARTICLE AS DOI: 10.1063/1.50240101

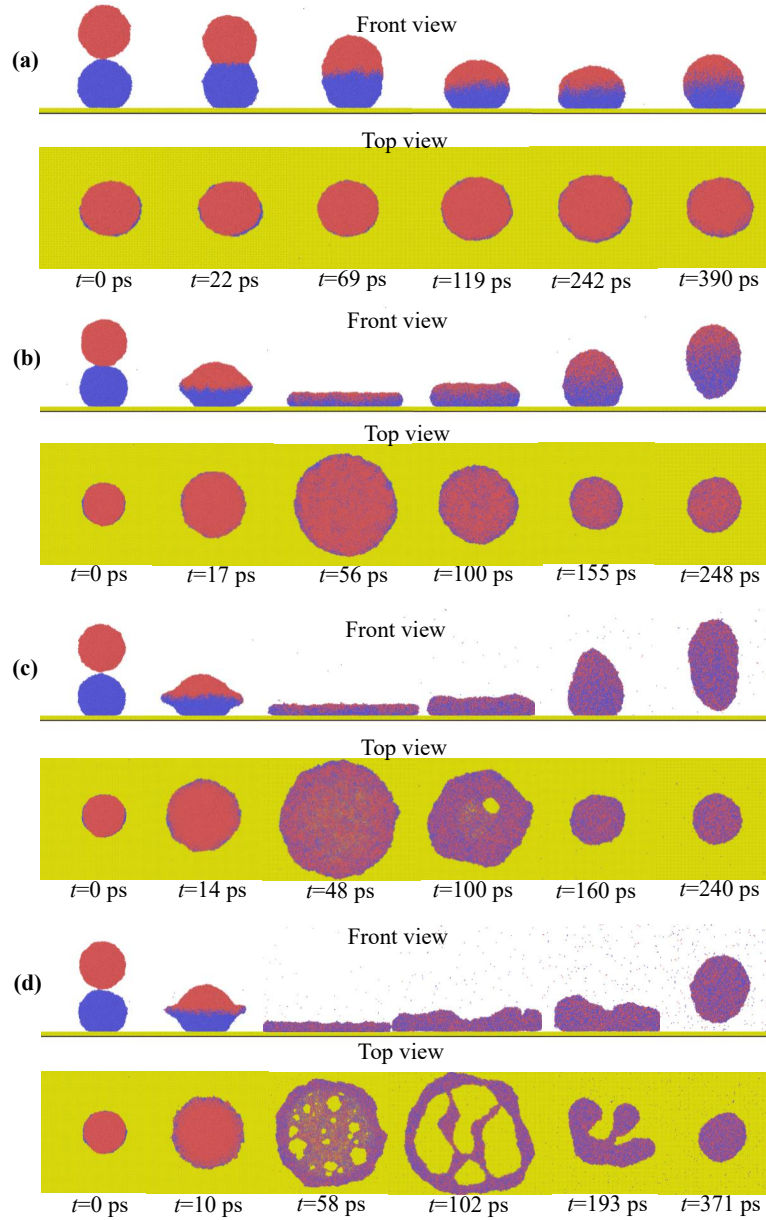


Fig. 4 Temporal evolutions of droplet profiles on the surface at $We =$ (a) 1.5, (b) 73.9, (c) 150.9, and (d) 217.3.

To demonstrate the impact of E_{vis} on droplet collisions, the restitution coefficients ($\varepsilon = v_j/v_i$, where v_j is the rebound velocity) under different We numbers were calculated, as shown in Fig. 5a. The maximum value of ε is only 0.1, indicating that the majority of the energy is dissipated in the form of E_{vis} , with only a small portion of the impact kinetic energy converted into the final rebound kinetic energy of the merged droplets. This finding is consistent with the conclusions of Ma et al.⁵² The value of ε is much lower than the results obtained at the macroscopic scale,⁴¹ because at the macroscopic scale, viscous dissipation only occurs in the boundary layer,⁵³⁻⁵⁶ whereas at the nanoscale, the velocity gradient extends throughout the entire droplet,^{19,57} significantly increasing viscous dissipation. This results in lower final rebound kinetic energy, particularly at lower We numbers, indicating that nanoscale collisions are more dissipative compared with their macroscopic counterparts. Fig. 5a also shows that as the We number increases, the ε first increases and then decreases. This is because, with the increase in impact kinetic energy, viscous dissipation does not increase as rapidly. To accurately represent the trend of viscous dissipation with impact velocity, the viscous dissipation energy is calculated according to

$$E_{\text{vis}} = E - E_m - E_s - E_w \quad (7)$$

Fig. 5b shows that viscous dissipation increases with increasing We number. However, based on the slope of the fitted line being 0.17, it can be seen that the rate of increase in viscous dissipation is much less than 1. Therefore, the ε gradually increases with the increase in We number. On the other hand, based on the ratio between viscous dissipation and initial kinetic energy ($E_{\text{vis}}/E_{k,0}$), it can be seen more clearly that this ratio rapidly decreases at lower We stages. However, when We exceeds 122.2, although the ratio of $E_{\text{vis}}/E_{k,0}$ has remained largely unchanged, it can be seen from Fig. 4c that holes start to appear at this point. Those holes lead to a loss of surface energy, which reduces the

kinetic energy available for the droplet to bounce back. As a result, the ε decreases rapidly as the number of holes increases.

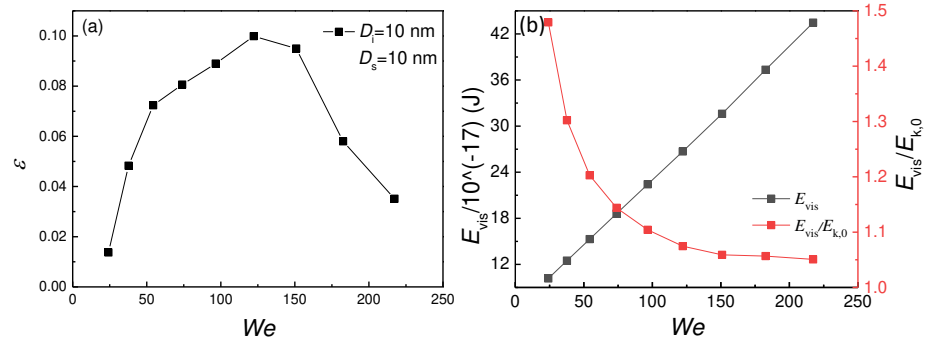


Fig. 5 (a) The relationship between the restitution coefficients ε and We for equal sized droplets of 10 nm. (b) The relationship between viscous dissipation E_{vis} , the ratio of viscous dissipation to initial kinetic energy $E_{vis}/E_{k,0}$, and We .

Fig. 6a presents the trend of the spreading coefficient ($\beta=D/D_i$) over time, showing that at all We numbers, β increases and then decreases with time. As the impact process progresses, both droplets start spreading simultaneously. After reaching maximum spreading, they gradually retract and eventually reach zero, bouncing off the surface. Fig. 6b shows that the maximum spreading coefficient increases with the We number.³⁵ The scaling law it follows will be discussed in detail in section 4.3. The time required to reach the maximum spreading diameter (t_{max}) is shown in Fig. 6c. When $We \leq 182.6$, t_{max} gradually decreases with increasing impact velocity, as the degree of droplet deformation increases and the spreading speed increases. However, Fig. 4d shows that many holes appear in the central region of the droplet during spreading, which actually increases t_{max} . For the contact time of the droplets (t_c , the time from when the impacting droplet just contacts the stationary droplet to when the merged droplet bounces off), as shown in Fig. 6d, it starts to increase at $We=150.9$.

This is the author's peer reviewed, accepted manuscript. However, the online version of record will be different from this version once it has been copyedited and typeset.

PLEASE CITE THIS ARTICLE AS DOI: 10.1063/1.50240101

This is because, at this We number, holes already appear during the droplet impact (Fig. 4c), causing t_j to increase. Therefore, the appearance of holes increases t_j , but only when holes appear during the spreading phase do they cause t_{max} to increase.

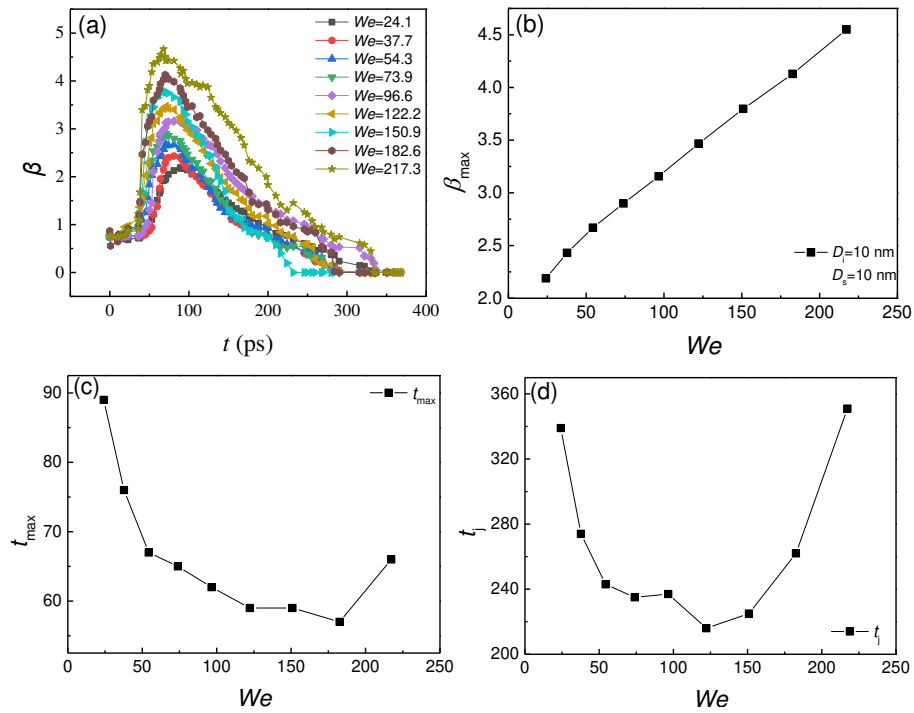


Fig. 6 (a) The evolutions of the spreading coefficient β for equal sized nanodroplet of 10 nm in a We range from 24.1 to 217.3. The relationship between (b) the maximum spreading coefficient β_{max} , (c) the maximum spreading diameter t_{max} , (d) the contact time t_j and We for equal sized nanodroplet of 10 nm.

4.2 Impact of unequal-sized droplets

This is the author's peer reviewed, accepted manuscript. However, the online version of record will be different from this version once it has been copyedited and typeset.
 PLEASE CITE THIS ARTICLE AS DOI: 10.1063/1.50240101

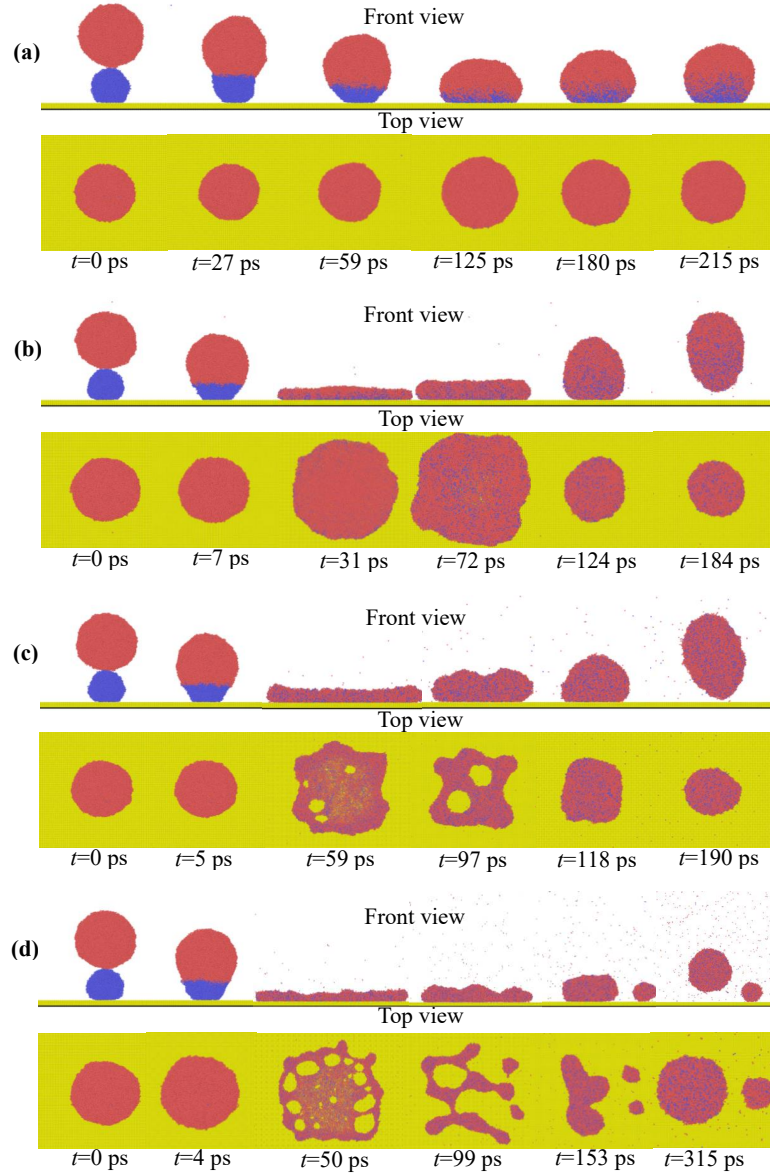


Fig. 7 Temporal evolutions of droplet profiles on the surface at $We =$ (a) 1.5, (b) 73.9, (c) 122.2, and (d) 150.9.

When considering unequal-sized droplet collisions, the diameter ratio ($\lambda=D_s/D_i$) significantly influences the collision outcomes. The present study explores the impact of varying the size of fixed droplets on a surface, with λ of 0.4, 0.6, and 0.8, during collision processes. At $We=1.5$ (low impact velocity), the collision process shown Fig. 7a is quite similar to the collision of droplets of equal size (Fig. 4a), and the droplets deposit on the surface after collision. As the impact velocity increases, the diameter ratio influences the collision outcome, causing the appearance of holes to occur earlier in the collision process. At $We=150.9$ with $\lambda=0.6$, numerous holes appear during the spreading phase, and the droplets eventually break up into two rebounding droplets (Fig. 7d). In contrast, under the same We number, droplets of equal size form only one hole during the retraction phase and eventually retract into a single rebounding droplet (Fig. 4c).

Further evidence of the influence of λ on droplet collision is presented in Fig. 8a. By comparing the variations of ε with We numbers under four different diameter ratios, it is observed that, similar to the collision of equal-sized droplets, ε initially increases and then decreases. The increase is attributed to $E_{vis}/E_{k,0}$, which first rapidly decreases and then basically unchanged with the We number (Figs. 5b and 8b). While at higher We values, the decrease of ε is due to the loss of surface energy caused by the appearance of holes, similar to the discussion in Section 4.1. Additionally, as λ decreases, ε gradually increases (Fig. 8a), indicating that a smaller diameter of the fixed droplet favors droplet rebound. Comparing E_{vis} at $\lambda=0.6$ and 1.0 (Fig. 8b), it is evident that the reduction in λ leads to decreased E_{vis} , thus increasing the kinetic energy available for rebound (E_j). The reduction in E_{vis} can be attributed to the decrease in contact time during the collision, as shown in Fig. 8c. At a diameter ratio of 1.0, the contact time for all We conditions is greater than that for other values at the same impact velocity. According to Equation 8, E_{vis} is directly proportional to contact time. Therefore, the

This is the author's peer reviewed, accepted manuscript. However, the online version of record will be different from this version once it has been copyedited and typeset.

PLEASE CITE THIS ARTICLE AS DOI: 10.1063/1.50240101

increase in contact time with increasing diameter ratio is the fundamental reason for the increase in

$E_{vis}^{.58}$

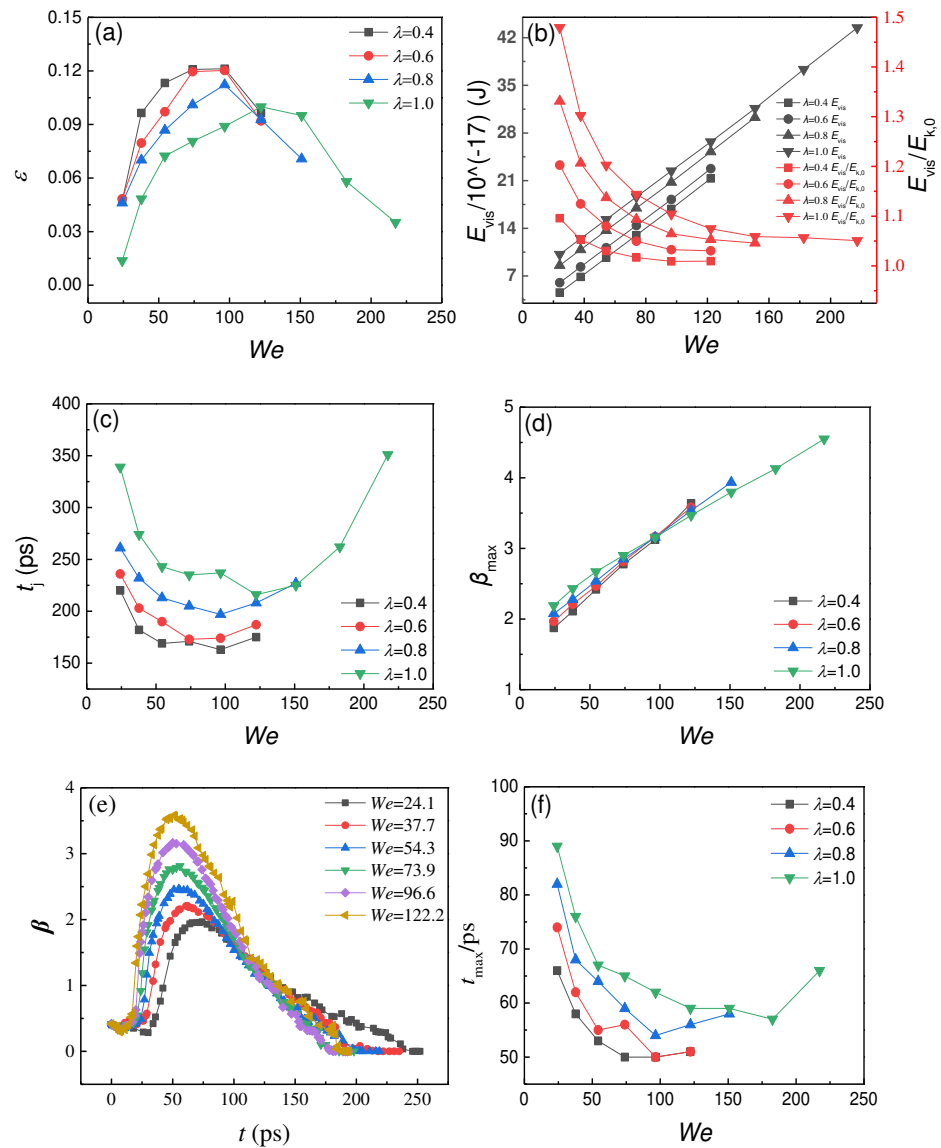


Fig. 8 (a) The relationship between the restitution coefficients ϵ and We for various λ . (b) The

relationship between viscous dissipation E_{vis} , the ratio of viscous dissipation to initial kinetic energy $E_{vis}/E_{k,0}$, and We for various λ . (c) The relationship between the contact time t_j and We for various λ . (d) The relationship between the maximum spreading coefficient β_{max} and We for various λ . (e) The evolutions of the spreading coefficient β for various λ in a We range from 24.1 to 122.2. (f) The relationship between the maximum spreading diameter t_{max} and We for various λ .

Although the maximum spreading diameter of droplets varies under different λ (Fig. 8d), the difference is relatively small compared with the significant increase in contact time (Fig. 8c). The maximum spreading diameter increases with increasing We number. Using $\lambda=0.6$ as an example, the relationship between the spreading diameter and time for all rebounding cases is calculated, as shown in Fig. 8e. Similar to the collision of equal-sized droplets (Fig. 6a), after the droplets make contact, they spread, retract, and rebound, resulting in an initial increase followed by a decrease, with the peak value increasing with We number. The time required to reach the maximum spreading diameter is similar to the contact time, initially decreasing and then increasing with increasing We number (Fig. 8f). This is because the increase in impact velocity causes greater deformation of the colliding droplets, shortening the time to reach the maximum spreading diameter. However, at a certain impact velocity, holes appear during the spreading phase, leading to an increase in time. It is noteworthy that smaller diameter ratios cause holes to appear earlier, resulting in the earlier breakup of the liquid film into two or more droplets. This finding also suggests that λ not only affects the energy dissipation but also the dynamics of droplet spreading and retraction. These observations are consistent with the scaling laws proposed by Ma et al.,⁵² where they highlighted that nanoscale droplet collisions are governed by different scaling relationships compared with macroscopic droplets.

4.3 Universal scaling laws of the impact of binary droplets

This is the author's peer reviewed, accepted manuscript. However, the online version of record will be different from this version once it has been copyedited and typeset.

PLEASE CITE THIS ARTICLE AS DOI: 10.1063/1.50240101

When a single nanoscale droplet impacts a surface, the contact time remains relatively constant at higher Weber numbers, following the scaling relationship $t \sim \tau_c = (D_i/\nu_i)We^{2/3}Re^{-1/3}$,¹⁹ which differs from the macroscopic scaling relationship $\tau \sim (\rho D_i^3/\gamma)^{1/2} = (D_i/\nu_i)We^{1/2}$.⁵⁹ At the nanoscale, viscous dissipation becomes non-negligible, meaning that contact time is influenced not only by the Weber number but also by the Reynolds number (Re). The question arises: during the collision of two nanoscale droplets, does the contact time follow the same scaling relationship as that of a single droplet?

To investigate this, we first define $t^* = t/(D_i/\nu_i)$ in a similar manner and extract the data from Fig. 8c, where the contact time remains relatively unchanged, for validation of the scaling relationship. As shown in Fig. 9a, the distribution of contact times is scattered, indicating that when two droplets of different diameters collide, the contact time does not conform to the scaling relationship observed in single nanoscale droplet impacts. This discrepancy arises because the diameter ratio plays a significant role during the collision, which must be taken into account.

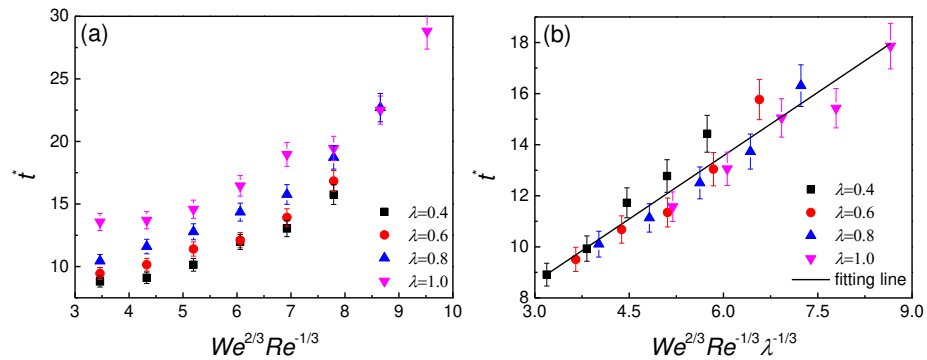


Fig. 9 (a) The relationship between the dimensionless contact time t^* and $We^{2/3}Re^{-1/3}$. (b) Revised dimensionless contact time t^* as a function of $We^{2/3}Re^{-1/3}\lambda^{-1/3}$ for various λ , fitted with a power-law $t^* \sim We^{2/3}Re^{-1/3}\lambda^{-1/3}$.

To address this discrepancy, the We and Re numbers are redefined as $We^* = We/\lambda$, $Re^* = Re/\lambda$.⁶⁰⁻⁶² The new scaling relationship becomes $t \sim (D_i/v_i) We^{*2/3} Re^{*-1/3} = (D_i/v_i) We^{2/3} Re^{-1/3} \lambda^{-1/3}$ that more accurately describes the dynamic behavior of droplet collisions under varying diameter ratios. This new scaling law effectively captures the influence of λ on collision dynamics, providing a more comprehensive framework for understanding droplet interactions at the nanoscale. After validating all the contact times under different conditions using the new scaling, it has been found that all the data aligns along a single straight line, as shown by the fitted line in Fig. 9b, thus confirming the correctness of the new scaling relationship.

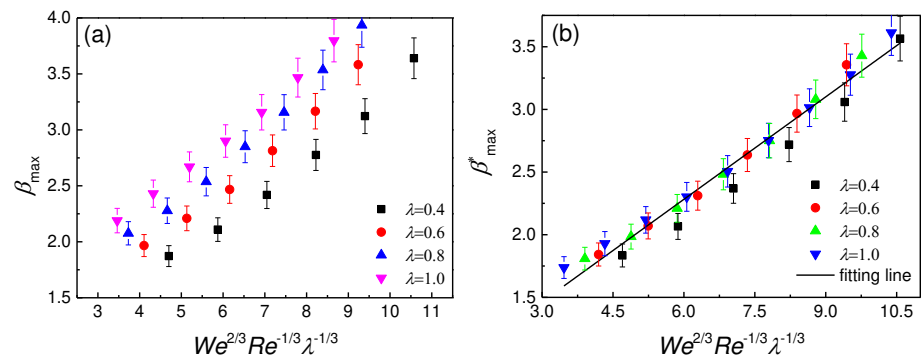


Fig. 10 (a) The relationship between the maximum spreading factor β_{\max} and $We^{2/3} Re^{-1/3} \lambda^{-1/3}$. (b) Revised the maximum spreading factor β^*_{\max} as a function of $We^{2/3} Re^{-1/3} \lambda^{-1/3}$ for various λ , fitted with a power-law $\beta^*_{\max} \sim We^{2/3} Re^{-1/3} \lambda^{-1/3}$.

Wang et al.,³⁵ based on the scaling relationship followed by t , further demonstrated that the maximum spreading factor during the impact of a single nanoscale droplet on a surface follows a similar scaling relationship: $\beta_{\max} \sim We^{2/3} Re^{-1/3}$. Following the same approach for handling the impact time of droplets with unequal sizes, if substituting the newly We^* and Re^* into $We^{2/3} Re^{-1/3}$, the maximum spreading factor should also follow the new scaling relationship, i.e., $\beta_{\max} \sim We^{2/3} Re^{-1/3} \lambda^{-1/3}$.

When validating all β_{\max} values under different conditions according to the new scaling, as shown in Fig. 10a, the data are surprisingly scattered, indicating that this theory does not apply to the collision of two droplets of unequal sizes. However, it has also been observed that the slope of the data variation is generally consistent across different values. Therefore, we further corrected β_{\max} , defining $\beta_{\max}^* = D_{\max}/D_m$, where $D_m = (D_i^3 + D_s^3)^{1/3} = (1 + \lambda^3)^{1/3} D_i$. Intriguingly, all four sets of data collapse onto a single universal curve, thereby verifying this scaling.

The present study's findings challenge some traditional assumptions about droplet impact dynamics, particularly at the nanoscale. While classical theories, such as those by Clanet et al.,⁴³ have been successful in describing macroscopic droplet impacts, they fall short in accurately predicting nanoscale behaviors. The discrepancies arise primarily from the increased significance of surface forces and viscous dissipation at smaller scales, which are often underestimated in classical models.

The newly proposed scaling relationship in this study offers a novel approach to understanding nanoscale droplet collisions by taking into account the unique characteristics of energy dissipation and spreading dynamics at this scale. This contrasts with previous models that primarily focused on inertial-capillary or viscous regimes, without considering the crossover states that are prevalent in nanoscale collisions. The new model in this work not only provides new insights into the collision dynamics of nanodroplets but also proposes a refined theoretical framework that better aligns with the observed behaviors at the nanoscale. The findings highlight the importance of revisiting and potentially revising classical theories to accommodate the unique physical phenomena that emerge at smaller scales.

4. Conclusion

This is the author's peer reviewed, accepted manuscript. However, the online version of record will be different from this version once it has been copyedited and typeset.

PLEASE CITE THIS ARTICLE AS DOI: 10.1063/1.50240101

This study utilizes MD simulations to thoroughly explore the collision behavior of equal and unequal-sized nanodroplets on a flat surface, uncovering the dynamic processes and energy conversion mechanisms involved. By setting different Weber numbers and diameter ratios, the research examines the spreading, retraction, and rebound behaviors of droplets under various conditions. In collisions between droplets of equal size, it is found that as the Weber number increases, the droplets transition from deposition to rebound, undergoing noticeable spreading and retraction. A detailed energy analysis reveals that during droplet collisions, kinetic energy conversion into surface energy is modulated by viscous dissipation, particularly at the nanoscale. This study further correlates these findings with existing theories on nanoscale energy dissipation, providing a deeper understanding of the factors influencing rebound efficiency and scaling behavior.

In the case of collisions between droplets of different sizes, the diameter ratio significantly influences the collision process. As the diameter of the fixed droplet decreases, viscous dissipation reduces, allowing more collision energy to be converted into rebound kinetic energy, resulting in increased rebound velocity. The analysis shows that at smaller diameter ratios, the contact time is significantly shortened, as the smaller droplet diameter leads to faster film rupture and earlier droplet separation. Although the maximum spreading diameter increases with the Weber number, its variation is relatively small compared with the significant increase in contact time observed under different diameter ratios. Further investigation reveals that by redefining the Weber and Reynolds numbers and introducing a new scaling relationship, the dynamic behavior of droplet collisions under varying diameter ratios can be more accurately described.

In conclusion, this study elucidates the complex dynamics involved in nanodroplet collisions, proposing a novel scaling relationship for unequal-sized droplets. These findings not only advance

This is the author's peer reviewed, accepted manuscript. However, the online version of record will be different from this version once it has been copyedited and typeset.

PLEASE CITE THIS ARTICLE AS DOI: 10.1063/1.50240101

the understanding of nanoscale collisions but also offer practical insights for applications in fields like inkjet printing, anti-icing and self-cleaning technologies. For instance, in inkjet printing, precise control over droplet deposition is critical for achieving high-resolution outputs. The novel scaling laws and understanding of energy dissipation presented here can be used to optimize droplet behavior during the printing process, improving print quality and material efficiency. In the field of anti-icing and self-cleaning surfaces, the findings on droplet rebound and spreading dynamics are directly relevant. Specifically, the reduction in contact time and the effective dissipation of energy may enhance the performance of surfaces designed to repel water or prevent ice formation. By integrating these new scaling laws into surface design, engineers could develop more effective coatings that maintain functionality in extreme environmental conditions. Expanding the application of these results across other industries, such as coating technologies and microfluidics, presents opportunities for further innovation based on the nanoscale dynamics explored in this work. However, the limitations of the MD simulation approach, such as finite simulation time and computational constraints, may affect the accuracy and generalizability of the results. On the other hand, the study's reliance on simulations highlights the need for further experimental validation to confirm these scaling laws across different materials and environmental conditions. Additionally, in this study, we focused on cases where λ is less than or equal to 1. While this range of λ is relevant to many practical applications, exploring cases where λ exceeds 1 could reveal new insights into the dynamics of unequal-sized droplet collisions. Future research will focus on expanding the parameter space to investigate whether the same scaling laws apply when the stationary droplet is larger than the impacting droplet.

CRedit authorship contribution statement

Fangfang Xie: Investigation, Writing – original draft, Methodology, Conceptualization, Funding acquisition. **Hongzeng Xin:** Writing – original draft, Visualization, Data curation. **Qianyi Liu:** Writing – original draft, Formal analysis. **Zhiyin Yang:** Writing – review & editing. **Amirali Shateri:** Writing – review & editing. **Wenpeng Hong:** Writing – review & editing. **Mingjun Liao:** Writing – review & editing, Supervision, Project administration.

Declaration of Competing Interest

The authors declare that they have no known competing financial interests or personal relationships that could have appeared to influence the work reported in this paper.

Data availability

Data will be made available on request.

Acknowledgments

This study was financially supported by the National Natural Science Foundation of China (No. 52306074).

References

- ¹Y. Guo, H. S. Patanwala, B. Bognet, and A. W. K. Ma, “Inkjet and inkjet-based 3D printing: connecting fluid properties and printing performance,” *Rapid Prototyping J.* **23**, 3 (2017).
- ²S. Xue, X. Xi, Z. Lan, R. Wen, and X. Ma, “Longitudinal drift behaviors and spatial transport efficiency for spraying pesticide droplets,” *Int. J. Heat Mass Transfer* **177**, 121516 (2021).
- ³J. Shi, B. Wu, J. Zhuo, D. Ren, D. Zhang, C. An, and J. Wang, “One-step rapid preparation of CL-20/TNT co-crystal assembly and spheroidized coating based on droplet microfluidic technology,” *Def. Technol.* **27**, 251 (2023).
- ⁴A. Khain, T. V. Prabha, N. Benmoshe, G. Pandithurai, and M. Ovchinnikov, “The mechanism of first

This is the author's peer reviewed, accepted manuscript. However, the online version of record will be different from this version once it has been copyedited and typeset.

PLEASE CITE THIS ARTICLE AS DOI: 10.1063/5.0240101

- raindrops formation in deep convective clouds,” *J. Geophys. Res-Atoms.* **118**, 9123 (2013).
- ⁵X. Yuan and Z. Xiong, “High frequency pulsed electrohydrodynamic printing with controllable fine droplets,” *J. Micromech. Microeng.* **28**, 095008 (2018).
- ⁶X. Zhang and L. Xiong, “Effect of adjuvants on the spray droplet size of pesticide dilute emulsion,” *Colloids Surf. Physicochem. Eng. Aspects* **619**, 126557 (2021).
- ⁷Q. Ma, Y. F. Wang, Y. B. Wang, X. He, S. F. Zheng, Y. R. Yang, X. D. Wang, and D. J. Lee, “Phase diagram for nanodroplet impact on solid surfaces,” *Phys. Fluids* **33**, 102007 (2021).
- ⁸Q. Zhang, T. Z. Qian, and X. P. Wang, “Phase field simulation of a droplet impacting a solid surface,” *Phys. Fluids* **28**, 022103 (2016).
- ⁹R. K. Singh, P. D. Hodgson, N. Sen, and S. Das, “Effect of Surface Roughness on Hydrodynamic Characteristics of an Impinging Droplet,” *Langmuir* **37**, 3038 (2021).
- ¹⁰H. Aziz, M. M. Amrei, A. Dotivala, C. Tang, and H. V. Tafreshi, “Modeling Cassie droplets on superhydrophobic coatings with orthogonal fibrous structures,” *Colloids Surf. Physicochem. Eng. Aspects* **512**, 61 (2017).
- ¹¹B. He, S. Yang, Z. Qin, B. Wen, and C. Zhang, “The roles of wettability and surface tension in droplet formation during inkjet printing,” *Sci. Rep.* **7**, 11841 (2017).
- ¹²M. Zhang, J. Chen, J. Zhu, Z. Tao, and L. Qiu, “Hybrid manipulation of inkjet-printing deposition pattern of high particle concentration droplet by means of thermal and binary solvent effects,” *Int. J. Heat Mass Transfer* **223**, 125225 (2024).
- ¹³H. Ren, F. Yang, and C. Deng, “Head-on collision of binary nanodroplets on rough surfaces: Impact velocity dependent spreading dynamics,” *Appl. Surf. Sci.* **541**, 148426 (2021).
- ¹⁴P. R. Brazier-Smith, H. Caermtz, G. Lavergne, and Y. Biscos, “Experimental investigation of

This is the author's peer reviewed, accepted manuscript. However, the online version of record will be different from this version once it has been copyedited and typeset.

PLEASE CITE THIS ARTICLE AS DOI: 10.1063/5.0240101

- dynamic binary collision of ethanol droplets – a model for droplet coalescence and bouncing,” P. Roy. Soc. A-Math. Phy. **326**, 393 (1997).
- ¹⁵J. P. Estrade, H. Caerntz, G. Lavergne, and Y. Biscos, “Experimental investigation of dynamic binary collision of ethanol droplets – a model for droplet coalescence and bouncing,” Int. J. Heat Fluid Flow **20**, 486 (1999).
- ¹⁶M. Sommerfeld and L. Pasternak, “Advances in modelling of binary droplet collision outcomes in Sprays: A review of available knowledge,” Int. J. Multiphase Flow **117**, 182 (2019).
- ¹⁷W. Klauser, F. T. von Kleist-Retzow, and S. Fatikow, “Line Tension and Drop Size Dependence of Contact Angle at the Nanoscale,” Nanomaterials **12**, 369 (2022).
- ¹⁸Y. B. Wang, Y. F. Wang, Y. R. Yang, X. D. Wang, and M. Chen, “Spreading Time of Impacting Nanodroplets,” J. Phy. Chem. B **125**, 5630 (2021).
- ¹⁹F. F. Xie, S. H. Lv, Y. R. Yang, and X. D. Wang, “Contact Time of a Bouncing Nanodroplet,” J. Phy. Chem. Lett. **11**, 2818 (2020).
- ²⁰M. Zhao, Y. Zhao, W. Li, F. Yang, B. Chen, and X. Xu, “Molecular dynamics simulation on the merging movement of nanodroplets on materials surface,” Results in Phys. **33**, 105213 (2022).
- ²¹I. Malgarinos, N. Nikolopoulos, and M. Gavaises, “A numerical study on droplet-particle collision dynamics,” Int. J. Heat Fluid Flow **61**, 499 (2016).
- ²²Y. B. Wang, Y. F. Wang, S. Y. Wang, B. X. Zhang, Y. R. Yang, and X. D. Wang, “Impact of a nanodroplet on liquid surfaces” Phys. Fluids **36**, 3 (2024).
- ²³J. Yan, K. Yang, X. Zhang, and J. Zhao, “Analysis of impact phenomenon on superhydrophobic surfaces based on molecular dynamics simulation,” Comp. Mater. Sci. **134**, 8 (2017).
- ²⁴L. Pasternak, J. M. Mañas, and M. Sommerfeld, “Influence of droplet properties on the coating of

This is the author's peer reviewed, accepted manuscript. However, the online version of record will be different from this version once it has been copyedited and typeset.

PLEASE CITE THIS ARTICLE AS DOI: 10.1063/5.0240101

- free-falling spherical particles,” *At. Sprays* **31**, 37 (2021).
- ²⁵A. G. Islamova, S. A. Kerimbekova, N. E. Shlegel, and P. A. Strizhak, “Droplet-droplet, droplet-particle, and droplet-substrate collision behavior,” *Powder Technol.* **403**, 117371 (2022).
- ²⁶Y. Cheng, J. Li, J. Xu, and Y. Shen, “Numerical investigations of head-on collisions of binary unequal-sized droplets on superhydrophobic walls,” *Phys. Fluids* **33**, 3 (2021).
- ²⁷L. Qian, J. Lin, H. Cong, F. Zhuo, and F. Bao, “A Numerical Investigation on the Collision Behavior of Unequal-Sized Micro-Nano Droplets,” *Nanomaterials* **10**, 9 (2020).
- ²⁸Y. N. Dong, N. N. Han, X. J. Zhang, B. X. Zhang, J. Y. Wang, and X. He, “Fluid transportation by droplets impacting wettability-controlled surfaces at the nanoscale: a molecular dynamics simulation study,” *Microfluid Nanofluid* **26**, 101 (2022).
- ²⁹H. Cao, R. Hu, Y. F. Chen, C. Gui, and Z. Yang, “Regulating droplet impact dynamics of nanoparticle suspension: Phenomena, mechanisms, and implications,” *Phys. Fluids* **36**, 1 (2024).
- ³⁰G. Shakya, M. Cattaneo, G. Guerriero, A. Prasanna, S. Fiorini, and O. Supponen, “Ultrasound-responsive microbubbles and nanodroplets: A pathway to targeted drug delivery,” *Adv. Drug Del. Rev.* **206**, 115178 (2024).
- ³¹H. Mertaniemi, R. Forchheimer, O. Ikkala, and R. H. A. Ras, “Rebounding Droplet-Droplet Collisions on Superhydrophobic Surfaces: from the Phenomenon to Droplet Logic,” *Adv. Mater.* **24**, 5738 (2012).
- ³²Y. R. Zhang and K. H. Luo, “Regimes of Head-On Collisions of Equal-Sized Binary Droplets,” *Langmuir* **35**, 8896 (2019).
- ³³W. Liu, N. Li, Z. Sun, Z. Wang, and Z. Wang, “Molecular Dynamics Study on Regimes of Head-on Droplet Collision,” *Langmuir* **38**, 411 (2022).

This is the author's peer reviewed, accepted manuscript. However, the online version of record will be different from this version once it has been copyedited and typeset.

PLEASE CITE THIS ARTICLE AS DOI: 10.1063/5.0240101

- ³⁴V. Molinero and E. B. Moore, “Water Modeled As an Intermediate Element between Carbon and Silicon,” *J. Phys. Chem. B.* **113**, 4008 (2009).
- ³⁵Y. F. Wang, Y. B. Wang, X. He, B. X. Zhang, Y. R. Yang, X. D. Wang, and D. J. Lee, “Scaling laws of the maximum spreading factor for impact of nanodroplets on solid surfaces,” *J. Fluid Mech.* **937**, A12 (2022).
- ³⁶L. Zhan, H. Chen, H. Zhou, J. Chen, H. Wu, and L. Yang, “Droplet-particle collision dynamics: A molecular dynamics simulation,” *Powder Technol.* **422**, 118456 (2023).
- ³⁷B. X. Li, X. H. Li, and M. Chen, “Spreading and breakup of nanodroplet impinging on surface,” *Phys. Fluids* **29**, 012003 (2017).
- ³⁸S. Stephan, J. Staubach, and H. Hasse, “Review and comparison of equations of state for the Lennard-Jones fluid,” *Fluid Phase Equilibria* **523**, 112772 (2020).
- ³⁹A. L. Xing, B. J. Li, C. M. Jiang, and D. J. Zhao, “Simulation of coalescence dynamics of droplets on surfaces with different wettabilities,” *Phys. Fluids* **34**, 7 (2022).
- ⁴⁰S. Wildeman, C. W. Visser, C. Sun, and D. Lohse, “On the spreading of impacting drops,” *J. Fluid Mech.* **805**, 636 (2016).
- ⁴¹S. Ray, Y. Han, Z. Yue, H. Guo, C. Y. H. Chao, and S. Cheng, “New insights into head-on bouncing of unequal-size droplets on a wetting surface,” *J. Fluid Mech.* **983**, A25 (2024).
- ⁴²Y. F. Wang, Y. B. Wang, F. F. Xie, J. Y. Liu, S. L. Wang, Y. R. Yang, S. R. Gao, and X. D. Wang, “Spreading and retraction kinetics for impact of nanodroplets on hydrophobic surfaces,” *Phys. Fluids* **32**, 9 (2020).
- ⁴³C. Clanet, C. Béguin, D. Richard, and D. QuÉRÉ, “Maximal deformation of an impacting drop,” *J. Fluid Mech.* **517**, 199 (2004).

This is the author's peer reviewed, accepted manuscript. However, the online version of record will be different from this version once it has been copyedited and typeset.

PLEASE CITE THIS ARTICLE AS DOI: 10.1063/5.0240101

- ⁴⁴S. Kim, "Collision of Polymer Nano Droplets: Molecular Dynamics Study," *Phys. Procedia* **34**, 66 (2012).
- ⁴⁵Y. Zhou, Z. Jin, and Z. Yang, "Effects of surface tension and viscosity on the impact process of droplets onto a rotational surface," *Phys. Fluids* **36**, 7 (2024).
- ⁴⁶P. J. Graham, M. M. Farhangi, and A. Dolatabadi, "Dynamics of droplet coalescence in response to increasing hydrophobicity," *Phys. Fluids* **24**, 11 (2012).
- ⁴⁷D. Chen, T. Wang, L. Ming, M. Qiu, and Z. Lin, "Dynamic characteristics of moving droplets impacting sessile droplets with different Reynolds numbers," *Phys. Fluids* **34**, 11 (2022).
- ⁴⁸C. Tang, P. Zhang, and C. K. Law, "Bouncing, coalescence, and separation in head-on collision of unequal-size droplets," *Phys. Fluids* **24**, 2 (2012).
- ⁴⁹M. Abouelsoud and B. Bai, "Bouncing and coalescence dynamics during the impact of a falling drop with a sessile drop on different solid surfaces," *Phys. Fluids* **33**, 6 (2021).
- ⁵⁰D. Bartolo, C. Josserand, and D. Bonn, "Retraction dynamics of aqueous drops upon impact on non-wetting surfaces," *J. Fluid Mech.* **545**, 329 (2005).
- ⁵¹P. Dhar, S. Mishra, and D. Samanta, "Onset of rebound suppression in non Newtonian droplets post impact on superhydrophobic surfaces," *Phys. Rev. Fluids* **41**, 103303 (2019).
- ⁵²Q. Ma, Y. F. Wang, and Y. B. Wang, "Ring-bouncing induced by the head-on impact of two nanodroplets on superhydrophobic surfaces," *Phys. Fluids* **35**, 043013 (2023).
- ⁵³C. W. Visser, P. E. Frommhold, S. Wildeman, R. Mettin, D. Lohse, and C. Sun, "Dynamics of high-speed micro-drop impact: numerical simulations and experiments at frame-to-frame times below 100 ns," *Soft Matter* **11**, 1708 (2015).
- ⁵⁴C. Antonini, A. Amirfazli, and M. Marengo, "Drop Impact and Wettability: From Hydrophilic to

This is the author's peer reviewed, accepted manuscript. However, the online version of record will be different from this version once it has been copyedited and typeset.

PLEASE CITE THIS ARTICLE AS DOI: 10.1063/1.50240101

- Superhydrophobic Surfaces,” *Phys. Fluids* **24**, 102104 (2012).
- ⁵⁵T. Gilet and J. W. M. Bush, “Droplets bouncing on a wet, inclined surface,” *Phys. Fluids* **24**, 122103 (2012).
- ⁵⁶H. M. Huang and X. P. Chen, “Energetic analysis of drop’s maximum spreading on solid surface with low impact speed,” *Phys. Fluids* **30**, 022106 (2018).
- ⁵⁷X. H. Li, X. X. Zhang, and M. Chen, “Estimation of viscous dissipation in nanodroplet impact and spreading,” *Phys. Fluids* **27**, 052007 (2015).
- ⁵⁸F. F. Xie, G. Lu, X. D. Wang, and D. Q. Wang, “Enhancement of Coalescence-Induced Nanodroplet Jumping on Superhydrophobic Surfaces,” *Langmuir* **34**, 11195 (2018).
- ⁵⁹D. Richard, C. Clanet, and D. Quéré, “Contact Time of a Bouncing Drop,” *Nature* **417**, 811 (2002).
- ⁶⁰H. Zhang, X. Yi, Y. Du, R. Zhang, X. Zhang, F. He, F. Niu, and P. Hao, “Dynamic behavior of water drops impacting on cylindrical superhydrophobic surfaces,” *Phys. Fluids* **31**, 032104 (2019).
- ⁶¹É. Lorenceau, C. Clanet, and D. Quéré, “Capturing drops with a thin fiber,” *J. Colloid Interface Sci.* **279**, 192 (2004).
- ⁶²S. G. Kim, and W. Kim, “Drop impact on a fiber,” *Phys. Fluids* **28**, 042001 (2016).